C. R. Geoscience 344 (2012) 377–384

Contents lists available at SciVerse ScienceDirect

Comptes Rendus Geoscience

www.sciencedirect.com

Petrology, geochemistry

Early Permian extensional shearing of an Ordovician granite: The Saint-Eutrope "C/S-like" orthogneiss (Montagne Noire, French Massif Central)

Cisaillement en extension d'un granite ordovicien au Permien inférieur : l'orthogneiss de "type C/S" de Saint-Eutrope (Montagne Noire, Massif central français)

Pavel Pitra [a,*], Marc Poujol [a], Jean Van Den Driessche [a], Jean-Charles Poilvet [a,b], Jean-Louis Paquette [c]

[a] *Géosciences Rennes, UMR 6118, Université Rennes 1 and CNRS, 35042 Rennes cedex, France*
[b] *Laboratoire Chrono-environnement, UMR 6249, Université de Franche-Comté, 25030 Besançon, France*
[c] *Laboratoire Magmas et Volcans, Université Blaise-Pascal, UMR CNRS 6524, 63038 Clermont-Ferrand cedex, France*

ARTICLE INFO

Article history:
Received 30 April 2012
Accepted after revision 26 June 2012
Available online 4 August 2012

Presented by Jean Aubouin

Keywords:
Montagne Noire
Extensional tectonics
S/C mylonite
Orthogneiss
U-Pb geochronology
Variscan orogen
France

ABSTRACT

Dating the magmatic events in the Montagne Noire gneiss dome is a key point to arbitrate between the different interpretations of the Late Carboniferous–Early Permian tectonics in this southern part of the Variscan belt. The Saint-Eutrope orthogneiss crops out along the northern flank of the dome. We show that the protolith of this orthogneiss is an Ordovician granite dated at 455 ± 2 Ma (LA-ICP-MS U-Pb dating on zircon). This age is identical to that previously obtained on the augen orthogneiss of the southern flank, strongly suggesting that both orthogneiss occurrences have the same Ordovician protolith. The Saint-Eutrope orthogneiss experienced intense shearing along the Espinouse extensional detachment at ca. 295 Ma (LA-ICP-MS U-Pb-Th on monazite), an age close to that determined previously on mica by the ^{39}Ar-^{40}Ar method and contemporaneous with the emplacement age of the syntectonic Montalet granite farther to the west. This normal sense shearing reworked previous fabrics related to Variscan thrusting that can be still observed in the augen orthogneiss of the southern flank, and is responsible for the spectacular "C/S-like" pattern of the Saint-Eutrope orthogneiss. This work also shows that care is needed when dealing with C/S-type structures, since they can develop not only in syntectonic intrusions, but also in orthogneisses affected by an intense secondary deformation, at decreasing temperature.

Mots clés :
Montagne Noire
Tectonique extensive
Mylonite C/S
Orthogneiss
Géochronologie U-Pb
Orogène varisque
France

RÉSUMÉ

Dater les événements magmatiques dans le dôme gneissique de la Montagne Noire est un point-clé pour départager les différentes interprétations de la tectonique de la transition Carbonifère–Permien dans la partie méridionale de la chaîne varisque. L'orthogneiss de Saint-Eutrope affleure le long du flanc nord du dôme. Nous montrons que le protolithe de cet orthogneiss est un granite ordovicien daté à 455 ± 2 Ma (datation U-Pb par LA-ICP-MS sur zircon). Cet âge est identique à celui obtenu auparavant sur les orthogneiss œillés du flanc sud. Cela suggère fortement que les deux orthogneiss avaient un protolithe ordovicien commun. L'orthogneiss de Saint-Eutrope a été affecté par un intense cisaillement le long du détachement extensif d'Espinouse à ca. 295 Ma (datation U-Pb-Th par LA-ICP-MS sur

* Corresponding author.
E-mail address: pavel.pitra@univ-rennes1.fr (P. Pitra).

1631-0713/$ – see front matter
http://dx.doi.org/10.1016/j.crte.2012.06.002

monazite). Cet âge est proche de celui déterminé auparavant sur micas par la méthode ^{39}Ar-^{40}Ar et contemporain avec la mise en place du granite syntectonique du Montalet, situé plus à l'ouest. Ce cisaillement en faille normale a repris la fabrique antérieure, associée au chevauchement varisque et qui peut encore être observée dans les orthogneiss œillés du flanc sud. Il est responsable de l'apparence de l'orthogneiss de Saint-Eutrope, spectaculairement similaire aux granites C/S. Ce travail montre qu'il est important de traiter avec précaution des structures de type C/S, car elles peuvent se développer non seulement dans des intrusions syntectoniques, mais aussi dans des orthogneiss ayant subi une intense déformation secondaire, à température décroissante.

1. Introduction

The tectonic interpretation of the Montagne Noire gneiss dome remains disputed. Numerous divergent models have been proposed ranging from compressive anticline, through diapiric uplift, to extensional gneiss dome (Van Den Driessche and Brun, 1992). Although the debate remains active, it is behind the scope of the present paper to discuss in detail these structural models. Intense shearing deformation has been described along the northern flank of the dome for a long time, especially in the orthogneiss that crops out in this area (Latouche, 1968). We call this specific orthogneiss the "Saint-Eutrope orthogneiss", named after a 14th century chapel built on these rocks (Fig. 1). The texture of this orthogneiss led Latouche (1968) and Bogdanoff et al. (1984) to compare it to the "gneiss minuti" of the Gran Paradiso massif in the Alps. For Demange (1975), the protolith of this orthogneiss is comagmatic with that of the augen orthogneisses found on the southern flank of the Montagne Noire. Latouche (1968) and Demange (1975) related the deformation of the Saint-Eutrope orthogneiss to the compressive Variscan

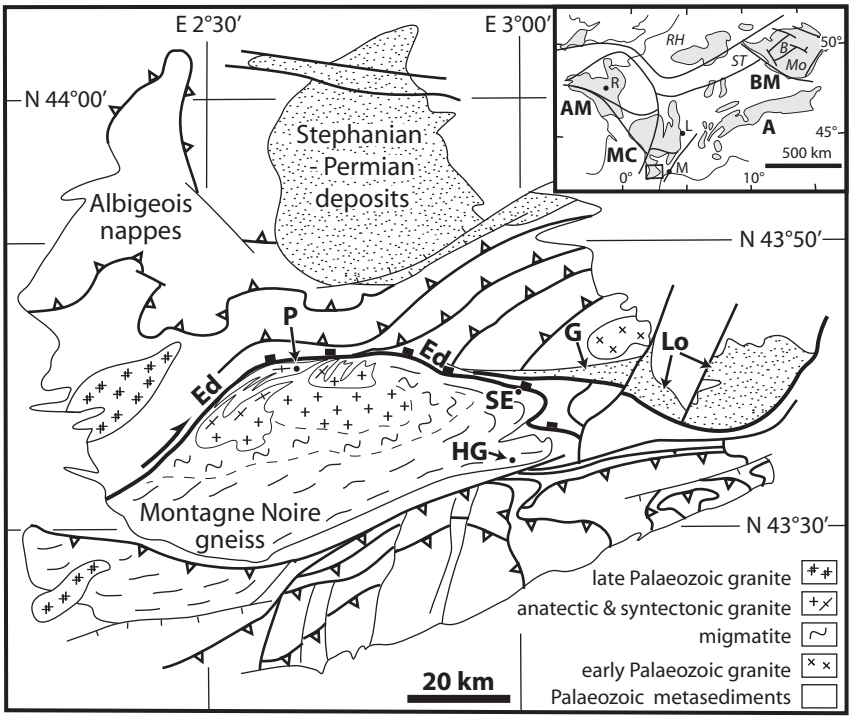

Fig. 1. Structural map of southern French Massif Central showing the relationships between the Montagne Noire gneiss dome, Late Carboniferous-Permian basins, and Variscan thrusts and nappes (modified after Brun and Van Den Driessche, 1994). Ed: Espinouse extensional detachment; G: Graissessac basin; HG: Héric gorges; Lo: Lodève basin; P: Col de Picotalen (location of the sample of the Montalet syntectonic leucogranite, Poilvet et al., 2011); SE: Saint-Europe chapel. Inset shows the location of the study area within the European Variscan belt (modified from Pitra et al., 2010). A: Alps; AM: Armorican Massif; BM: Bohemian Massif; MC: Massif Central; B: Teplá-Barrandian; Mo: Moldanubian; ST: Saxothuringian; RH: Rhenohercynian. L: Lyon, M: Montpellier, R: Rennes.

Fig. 1. Schéma structural du Sud du Massif central montrant les relations entre le dôme gneissique de la Montagne Noire, les bassins stéphano-permiens et les nappes et chevauchements varisques (modifié d'après Brun et Van Den Driessche, 1994). Ed : détachement d'Espinouse ; G : bassin de Graissessac ; HG : gorges d'Héric ; Lo : bassin de Lodève ; P : col de Picotalen (localisation de l'échantillon du leucogranite syntectonique de Montalet, Poilvet et al., 2011) ; SE : chapelle de Saint-Europe. L'encart montre la position de la zone d'étude dans la chaîne varisque européenne (modifié d'après Pitra et al., 2010). A : Alpes ; AM : Massif armoricain ; BM : Massif de Bohême ; MC : Massif central ; B : Teplá-Barrandien ; Mo : Moldanubien ; ST : Saxothuringien ; RH : Rhenohercynien. L : Lyon ; M : Montpellier ; R : Rennes.

tectonics. Beaud (1985), Van Den Driessche and Brun (1992) and Brun and Van Den Driessche (1994) interpreted this orthogneiss as a C/S mylonitic leucogranite emplaced within the detachment shear zone that would be responsible for the dome uplift during extensional tectonics. According to Gapais (1989), C/S structures (Berthé et al., 1979b) typically develop in syn-kinematic intrusions. During extension, the emplacement of granitic bodies within an extensional detachment zone is supposed to be fast enough (Davy et al., 1989) so that dating such bodies provides a close estimate for the age of the deformation. For this reason we decided to date the emplacement age of the Saint-Eutrope orthogneiss using the U-Th-Pb LA-ICP-MS method on both zircon and monazite.

2. Petrography and texture of the Saint-Eutrope orthogneiss

The Saint-Eutrope orthogneiss is a peraluminous, leucocratic, fine-grained (0.1–0.5 mm), locally porphyric, muscovite ± biotite-bearing granitic rock. It commonly contains large (up to 5 cm) porphyroclasts of K-feldspar (Fig. 2a). In some samples, tourmaline and garnet are present. The orthogneiss contains veins of tourmaline + muscovite-bearing pegmatites that have a foliation parallel to the main foliation of the orthogneiss. The main foliation is defined by flattening of feldspar, quartz-feldspar aggregates and shape preferred orientation of micas. K-feldspar porphyroclasts have Carlsbad twins and flame perthites. The porphyroclasts are in general also parallel to the rock foliation and asymmetric recrystallization tails developed on their short sides. Smaller equant grains formed by dynamic recrystallization at the rim of K-feldspar porphyroclasts. Quartz is mixed with other minerals and ribbons, if present, are short, without an internal grain shape orientation. Quartz grains are commonly equant or slightly elongated parallel to the foliation and their boundaries suggest bulging recrystallization (Fig. 2d). The foliation strikes east-west and dips about 20–30° N. The dominant structures are relatively pervasive discrete regular shear planes striking east-west and dipping ca. 40–50° N, about 20° steeper than the foliation (Fig. 2a, c, d). They bear fine striae plunging about 40° to the north-east

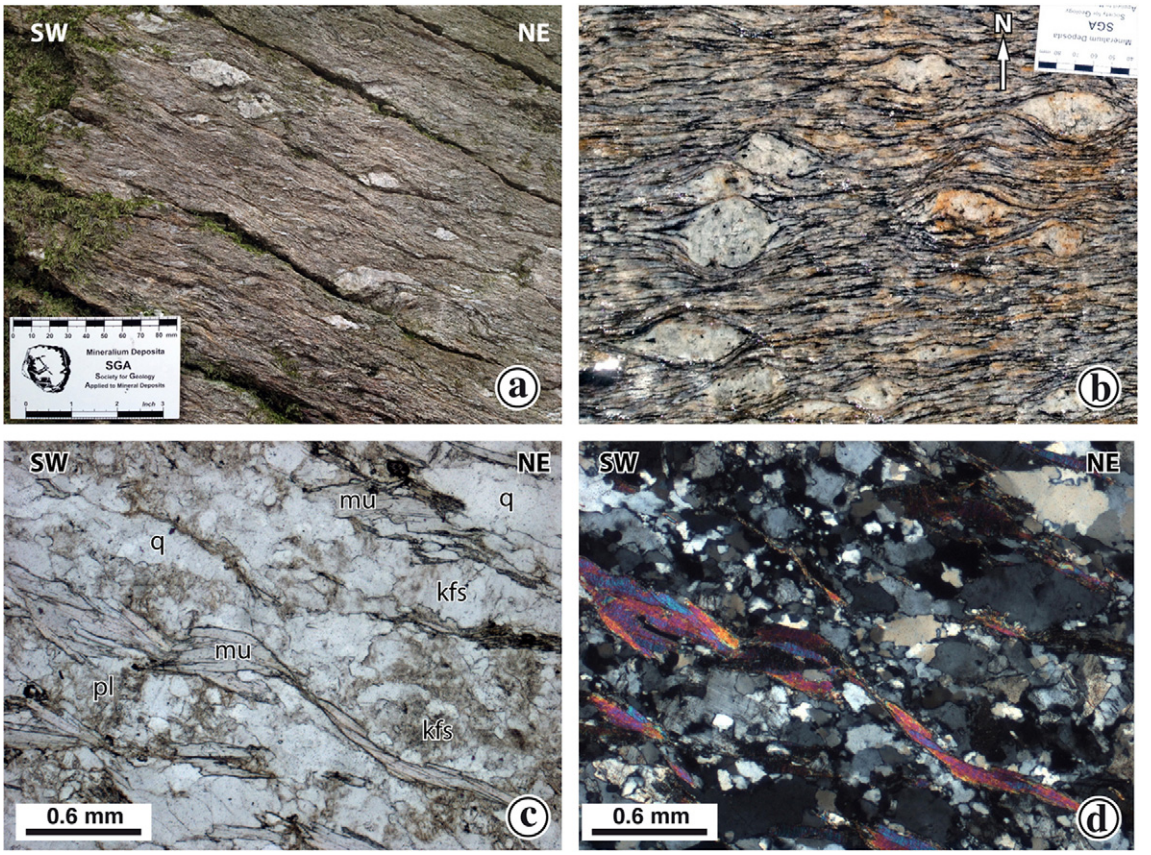

Fig. 2. a: outcrop photograph of the Saint-Eutrope orthogneiss displaying large porphyroclasts of K-feldspar, elongated parallel to the foliation, and conspicuous shear bands, indicating a normal movement to the north-east; b: outcrop photograph of the Héric gorges augen orthogneiss. The foliation is subvertical; c, d: photomicrographs of the Saint-Eutrope orthogneiss in PPL (c) and XPL (d). Muscovite (mu) is oriented parallel to S and locally affected by north-east dipping shear bands. Note the lack of quartz ribbons and grain-boundary migration recrystallization. kfs: K-feldspar; pl: plagioclase; q: quartz.

Fig. 2. a : affleurement de l'orthogneiss de Saint-Eutrope avec de grands porphyroclastes de feldspath K, allongés parallèlement à la foliation, et des bandes de cisaillement indiquant un mouvement normal vers le nord-est ; b : affleurement de l'orthogneiss œillé des gorges d'Héric. La foliation est subverticale ; c, d : photographies au microscope polarisant de l'orthogneiss de Saint-Eutrope en LPNA (c) et LPA (d). Les cristaux de muscovite (mu) sont parallèles à la foliation S et localement affectés par des bandes de cisaillement à pendage nord-est. Notez l'absence de rubans de quartz et de recristallisation par migration des joints de grains. kfs : feldspath K ; pl : plagioclase ; q : quartz.

Table 1
U-Pb LA-ICP-MS data for the zircon grains extracted from sample ES2.

Tableau 1
Données U-Pb obtenues par LA-ICP-MS sur des zircons de l'échantillon ES2.

Grain (zircon)	[Pb] (ppm)	[U] (ppm)	Th/U	$^{207}Pb/^{235}U$	± 1 σ	$^{206}Pb/^{238}U$	± 1 σ	$^{207}Pb/^{206}Pb$	± 1 σ	Rho	Ages				Conc. (%)
											$^{207}Pb/^{235}U$	$^{206}Pb/^{238}U$	$^{207}Pb/^{206}Pb$	± 1 σ	
1.1a	56	767	0.09	0.872	0.011	0.0899	0.0011	0.0703	0.0008	0.91	637	555	938	24	59
1.2a (*)	39	682	0.06	0.572	0.007	0.0732	0.0009	0.0567	0.0007	0.91	459	455	478	26	95
2a (*)	19	323	0.13	0.577	0.009	0.0736	0.0009	0.0569	0.0008	0.77	463	458	486	32	94
4a (*)	22	380	0.14	0.580	0.009	0.0735	0.0009	0.0572	0.0008	0.78	464	457	498	31	92
6a (*)	25	458	0.06	0.554	0.008	0.0710	0.0008	0.0566	0.0008	0.83	448	442	476	29	93
7.1a	36	400	0.18	0.992	0.013	0.1091	0.0013	0.0659	0.0008	0.90	700	668	805	24	83
8.1a	16	179	0.64	0.853	0.012	0.0979	0.0012	0.0632	0.0009	0.81	627	602	716	29	84
8.2a	19	367	0.13	0.528	0.008	0.0665	0.0008	0.0576	0.0009	0.74	430	415	515	33	81
10a (*)	33	588	0.06	0.559	0.007	0.0726	0.0009	0.0559	0.0007	0.88	451	452	447	26	101
12.1a	16	283	0.07	0.579	0.008	0.0711	0.0008	0.0591	0.0008	0.81	464	443	572	29	77
12.2a	25	323	0.51	0.888	0.012	0.0817	0.0010	0.0788	0.0010	0.84	645	506	1167	26	43
13a (*)	45	695	0.54	0.561	0.008	0.0730	0.0009	0.0558	0.0007	0.86	452	454	442	27	103
14.1a	34	657	0.07	0.527	0.007	0.0670	0.0008	0.0570	0.0007	0.84	430	418	491	29	85
14.2a (*)	14	245	0.11	0.569	0.009	0.0733	0.0009	0.0563	0.0008	0.78	458	456	465	32	98
15.2a	16	322	0.09	0.485	0.009	0.0629	0.0008	0.0559	0.0010	0.65	401	393	449	39	88
18.1a (*)	19	329	0.09	0.578	0.008	0.0740	0.0009	0.0566	0.0008	0.82	463	460	476	29	97
18.2a	17	212	0.15	0.835	0.012	0.1002	0.0012	0.0604	0.0008	0.82	616	615	619	29	99
19a	21	351	0.17	0.618	0.011	0.0752	0.0009	0.0596	0.0010	0.68	489	467	591	36	79
20.1a	34	301	0.27	1.223	0.016	0.1344	0.0016	0.0660	0.0008	0.86	811	813	806	26	101
21.1a	32	254	0.53	1.289	0.018	0.1385	0.0016	0.0675	0.0009	0.82	841	836	853	27	98
24a (*)	15	255	0.07	0.563	0.009	0.0727	0.0009	0.0562	0.0008	0.74	454	452	460	33	98
27a (*)	32	520	0.28	0.565	0.008	0.0732	0.0009	0.0560	0.0007	0.83	455	455	451	29	101
29a (*)	8	140	0.23	0.567	0.010	0.0726	0.0009	0.0566	0.0010	0.67	456	452	476	38	95
31a (*)	28	472	0.24	0.555	0.008	0.0708	0.0008	0.0568	0.0008	0.81	448	441	485	30	91
34a (*)	12	207	0.06	0.582	0.010	0.0753	0.0009	0.0561	0.0009	0.68	466	468	457	37	102

Grains marked (*) are those used for the calculation of the concordia age of 455 Ma.

(Figs. 4 and 5 in Van Den Driessche and Brun, 1992 for detailed structural maps). This indicates shear deformation associated with a normal movement to the north-east. Locally, the foliation is nearly parallel to the shear planes and the development of steep shear bands can then be observed, consistent with the normal sense of shear. The analysed sample was taken near the Saint-Eutrope chapel (43°39′41.48″N, 2°59′20.27″E).

The rock bears textural similarities with a syntectonic C/S granite, but the presence of K-feldspar augen, uncommon in such context, suggests that it may rather be a porphyric orthogneiss re-deformed in a ductile normal shear zone. The lack of quartz ribbons displaying an internal shape fabric and grain-boundary migration recrystallization, typical of C/S granitoids (Berthé et al., 1979a; Gapais and Barbarin, 1986; Pitra et al., 1994), also points towards this interpretation.

3. U-Th-Pb LA-ICP-MS dating

3.1. Analytical techniques

A classic mineral separation procedure has been applied to concentrate minerals suitable for U-Th-Pb dating using the facilities available at Géosciences Rennes. Rocks were crushed and only the powder fraction with a diameter less than 250 μm has been kept. Heavy minerals were successively concentrated by Wilfley table and heavy liquids. Magnetic minerals were then removed with an isodynamic Frantz separator. Zircon and monazite grains were carefully handpicked under a binocular microscope and embedded in epoxy mounts. The grains were then hand-grounded and polished on a lap wheel with a 6 μm and 1 μm diamond suspension successively. Zircons were imaged by cathodoluminescence (CL) using a Reliotron CL system equipped with a digital colour camera available at Géosciences Rennes.

U-Th-Pb geochronology of zircon and monazite was conducted by in situ laser ablation inductively coupled plasma mass spectrometry (LA-ICP-MS) at the Laboratoire Magmas et Volcans in Clermont-Ferrand, France. Ablation spot diameters of 26 μm and 7 μm with repetition rates of 3 Hz and 1 Hz were used for zircon and monazite, respectively. Data were corrected for U-Pb and Th-Pb fractionation and for the mass bias by standard bracketing with repeated measurements of the 91500 zircon (Wiedenbeck et al., 1995) or the Moacyr monazite standards (Gasquet et al., 2010). Repeated analyses of GJ-1 zircon (Jackson et al., 2004) or Manangoutry monazite (Paquette and Tiepolo, 2007) standards treated as unknowns were used to control the reproducibility and accuracy of the corrections. Data reduction was carried out with the GLITTER® software package developed by the Macquarie Research Ltd. (Jackson et al., 2004). Concordia ages and diagrams were generated using Isoplot/Ex (Ludwig, 2001). All errors given in Tables 1 and 2 are listed at one sigma, but where data are combined for regression analysis or to calculate weighted means, the final results are provided with 95% confidence limits. Further information on the instrumentation and the analytical technique is detailed in Hurai et al. (2010).

Table 2
U-Th-Pb LA-ICP-MS data for the monazite grains extracted from sample ES2.

Tableau 2
Données U-Th-Pb obtenues par LA-ICP-MS sur des monazites de l'échantillon ES2.

Grain	[Pb] (ppm)	[U] (ppm)	[Th] (ppm)	Th/U	$^{206}Pb/^{238}U$	±(1σ)	$^{207}Pb/^{235}U$	±(1σ)	$^{208}Pb/^{232}Th$	±(1σ)	Ages			
											$^{206}Pb/^{238}U$	$^{207}Pb/^{235}U$	$^{208}Pb/^{232}Th$	±(1σ)
06120410c	1171	2464	79,494	32	0.04862	0.00058	0.36096	0.00686	0.0146	0.0001	306	313	293	3
07120410c	1067	3143	69,358	22	0.04849	0.00057	0.34415	0.00625	0.0147	0.0001	305	300	296	3

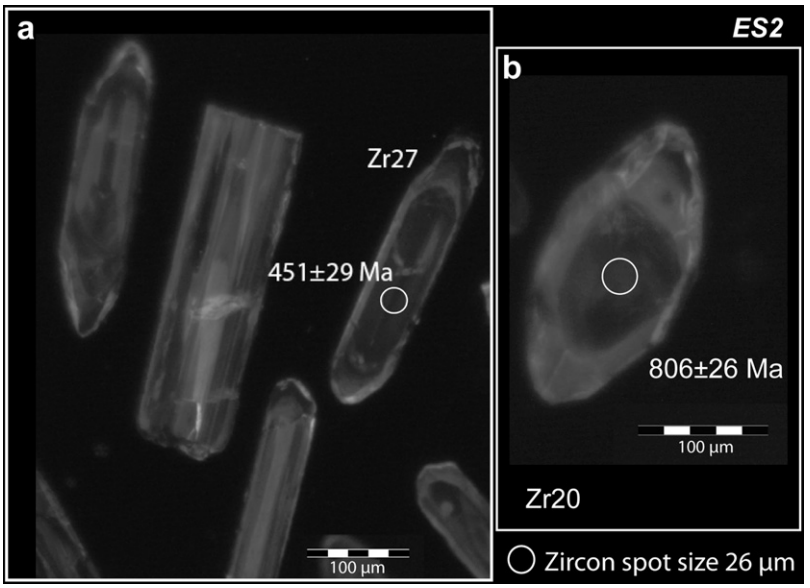

Fig. 3. Cathodoluminescence images of some of the zircon grains dated in this study: a: euhedral and elongated crystals with nicely defined magmatic zoning; b: euhedral squat crystals with evidence of inherited dark cores surrounded by brighter rims. The white circles represent the spot analyses and the numbers correspond to the $^{207}Pb/^{206}Pb$ ages found. Zr number corresponds to the grain number in Table 1.

Fig. 3. Photographies en cathodoluminescence de certains des zircons datés lors de cette étude : a : cristaux allongés et automorphes avec une zonation magmatique bien développée ; b : cristaux trapus automorphes avec des évidences de cœurs sombres hérités, entourés par des bordures plus claires. Les cercles blancs représentent la position des analyses ponctuelles et les chiffres correspondent aux âges $^{207}Pb/^{206}Pb$ trouvés. Les numéros Zr correspondent aux numéros des grains dans le Tableau 1.

3.2. Results

Numerous zircon and only two monazite grains were recovered from this sample. Zircons were usually lightly pink, euhedral and elongated with nicely defined magmatic zoning (Fig. 3a). Some, however, were euhedral squat grains with inherited dark cores surrounded by brighter rims (Fig. 3b). Monazite grains were subhedral and slightly yellow in colour.

Twenty-five analyses were performed on 20 zircon grains (Table 1). Plotted in a Tera-Wasserburg concordia diagram (Fig. 4a), zircon grains plot on a concordant to discordant position with apparent dates ranging from ca. 810 Ma down to 400 Ma. Two groups of ellipses (shaded)

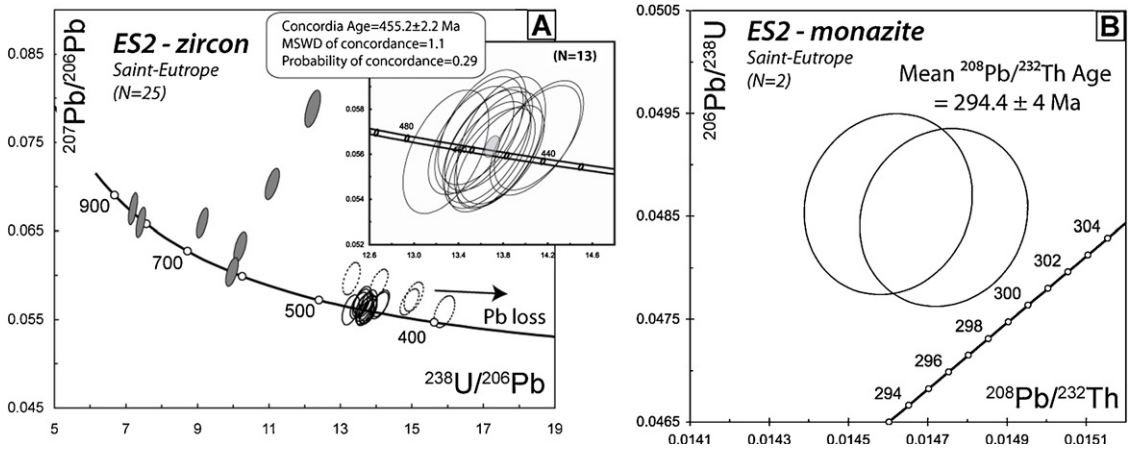

Fig. 4. A. Tera-Wasserburg $^{207}Pb/^{206}Pb$ versus $^{238}U/^{206}Pb$ concordia diagram for zircons analyzed in this study. Inset: close-up for the thirteen concordant points. B. $^{206}Pb/^{238}U$ versus $^{208}Pb/^{232}Th$ diagram for the monazite analyzed in this study. N refers to the number of analyses. All ellipses are represented at one sigma level. All ages are quoted at two sigma level.

Fig. 4. A. Diagramme concordia de Tera-Wasserburg $^{207}Pb/^{206}Pb$ vs $^{238}U/^{206}Pb$ pour les zircons analysés dans cette étude. L'encart montre un agrandissement pour les treize points concordants. B. Diagramme $^{206}Pb/^{238}U$ vs. $^{208}Pb/^{232}Th$ pour les monazites analysées dans cette étude. N correspond au nombre d'analyses. Toutes les ellipses d'erreur sont représentées à un sigma. Tous les âges sont donnés à deux sigmas.

define two dates, ca. 810 Ma and 620 Ma, respectively. A group of thirteen concordant points (unfilled ellipses) allows one to calculate a concordia date (Ludwig, 1998) of 455.2 ± 2.2 Ma (Fig. 4a insert, grey-filled ellipse). The position of the dash-lined ellipses (Fig. 4a) can be attributed to variable degrees of Pb loss.

The two monazite grains have been analysed (Table 2). In a $^{206}Pb/^{238}U$ versus $^{208}Pb/^{232}Th$ concordia diagram (Fig. 4b), they plot in a slightly reverse discordant position, which could be attributed to excess ^{206}Pb due to excess ^{230}Th as described by Schärer (1982). To avoid calculating an artificially older age if ^{206}Pb excess is confirmed, we favour dealing with the $^{208}Pb/^{232}Th$ ratios. They allow to calculate a mean $^{208}Pb/^{232}Th$ date of 294.4 ± 4 Ma.

4. Interpretation and geological significance of the geochronological data

Two interpretations can be drawn from the geochronological data. Either all zircon grains are inherited and monazite dates the emplacement and the contemporaneous deformation of the rock, or the date of ca. 455 Ma yields the age of emplacement of the protolith and monazite dates a subsequent deformation event at ca. 294 Ma. Two arguments are in favour of the second hypothesis. First, in the syntectonic Montalet leucogranite (Poilvet et al., 2011), emplaced along the Espinouse detachment farther west, not only monazite but also zircon crystallized from the magma during the emplacement, and the same behaviour would be expected if the Saint-Eutrope orthogneiss was a syntectonic intrusion. Second, as argued before, the porphyric character of the Saint-Eutrope orthogneiss is not expected in syntectonic leucogranites. Therefore, we interpret the concordant date of 455.2 ± 2.2 Ma, yielded by a large proportion of the analysed zircon grains, as the age of the emplacement of the orthogneiss protolith. This age is identical to the mean average $^{207}Pb/^{206}Pb$ age of 455 ± 2 Ma found for the protolith of the augen orthogneisses from the southern flank of the Montagne Noire dome (Roger et al., 2004). This agrees with the comagmatic origin of these orthogneisses, as previously suggested by Demange (1975). It also implies that the rocks from the Saint-Eutrope locality, despite the textural resemblance, are not a syntectonic leucogranite as proposed by Beaud (1985), Van Den Driessche and Brun (1992) and Brun and Van Den Driessche (1994), but instead an orthogneiss reactivated in a ductile normal shear zone. The ductile extensional shearing was sufficiently intense to strongly rework the previous fabrics that developed during the Variscan compressive tectonics and that can be still observed in the orthogneisses of the southern flank, unaffected by the extensional shearing (Héric gorges, Figs. 1, 2b). The same orthogneiss displays therefore a strikingly contrasting deformation imprint on the northern and southern flank of the Montagne Noire dome, respectively. This asymmetric character of the deformation at the scale of the dome is characteristic for detachment-controlled gneiss domes developed in extensional settings (Brun and Van Den Driessche, 1994; Brun et al., 1994; Buck, 1988; Davis and Coney, 1979; Wernicke and Axen, 1988) and supports this interpretation for the origin of the Montagne Noire gneiss dome (Van Den Driessche and Brun, 1992). This interpretation is also consistent with the Late Carboniferous post-thickening LP-HT metamorphism, which caused partial melting in the core of the Montagne Noire gneiss dome and with the subsequent exhumation of the dome below the Espinouse detachment (Brun and Van Den Driessche, 1994).

In order to understand the C/S character of the Saint-Eutrope orthogneiss, one may remember that true pervasive C/S structures only develop during retrograde deformation histories (Gapais, 1989). This is typically the case for syntectonic intrusions, but should also apply to hot orthogneisses deformed subsequently at decreasing temperature. This would explain the "C/S-like" mesoscopic deformation patterns observed in the Saint-Eutrope orthogneiss (Fig. 2). Moreover the presence of K-feldspar augen in a granitoid is symptomatic of a two-stage crystallisation process that is rather difficult to conciliate with the rapid emplacement and cooling of a syntectonic leucogranite during an extensional tectonic event. This confirms that C/S structures are not exclusively indicative of syntectonic intrusions.

Since the date of 455 Ma is considered as the age of the Saint-Eutrope granitic protolith, the dates of ca. 810 Ma and 620 Ma are interpreted as the ages of the source material inherited in the original granite. This inheritance can be attributed either to a Proterozoic basement or to sediments, which recycled such a basement. As the Saint-Eutrope orthogneiss is muscovite-bearing, the protolith was probably a S-type granite. Therefore we favour a sedimentary inheritance, although the presence of a Proterozoic basement cannot be completely ruled out.

Although the zircons did not record any younger event (as in Roger et al., 2004), two monazite grains allowed to calculate a mean $^{208}Th/^{232}Pb$ date of 294.4 ± 4 Ma. This date is interpreted as the age of the deformation (and probable associated fluid circulation) of the protolith of the Saint-Eutrope orthogneiss along the Espinouse detachment. This age agrees within the uncertainty with the 297 ± 2.8 Ma obtained on muscovite extracted from the same orthogneiss (Maluski et al., 1991) and interpreted as marking the end of the ductile normal movement. This age is also identical to the 294.4 ± 2.6 Ma dating the emplacement of the C/S syntectonic Montalet leucogranite (Brun and Van Den Driessche, 1994; Poilvet et al., 2011), emplaced along the Espinouse detachment farther to the west (Fig. 1). Finally, Bruguier et al. (2003) published an age of 295 ± 5 Ma for zircons extracted from a volcanic ash layer interbedded in the Late Carboniferous–Early Permian sedimentary fill of the Graissessac-Lodève basin. This hemi-graben is situated immediately to the northeast of the Saint-Eutrope orthogneiss, in the hanging wall of the Espinouse detachment (Fig. 1). The contemporaneity of ductile deformation in the basement and deposition of the ash layer confirms that the Espinouse detachment controlled the development of the basin (Van Den Driessche and Brun, 1989; Becq-Giraudon and Van Den Driessche, 1993), which is best explained by the interpretation of the Montagne Noire in the framework of large scale crustal extension.

5. Conclusion

The protolith of the Saint-Eutrope orthogneiss from the northern flank of the Montagne Noire is an Ordovician granitic intrusion emplaced 455 ± 2 Ma ago. This protolith

age is identical to that of the augen orthogneisses from the southern flank, suggesting that they are comagmatic. However, deformation patterns differ between the two occurrences; the C/S patterns are only found within the Saint-Eutrope orthogneiss. They are related to the intense normal shearing that took place ca. 295 Ma ago along the Espinouse detachment and that did not affect the southern part of the Montagne Noire dome. This asymmetric character of the deformation at the scale of the dome is characteristic for detachment-controlled gneiss domes developed in extensional settings, supporting this interpretation for the Montagne Noire. Finally, this work also shows that care is needed when dealing with C/S-type structures, since they can develop not only in syntectonic intrusions, but also in orthogneisses affected by an intense later deformation at decreasing temperature.

Acknowledgments

We are indebted to Jean-Pierre Burg and an anonymous reviewer for swift and constructive reviews. Marc Chaussidon is thanked for his efficient editorial handling of the manuscript.

References

Beaud F., 1985. Étude structurale de la zone axiale orientale de la Montagne Noire (sud du Massif central français) : détermination des mécanismes de déformation; relation avec les nappes du versant sud. Thèse 3e cycle, université Montpellier 2, 196 p.

Becq-Giraudon, J.F., Van Den Driessche, J., 1993. Continuité de la sédimentation entre le Stéphanien et l'Autunien dans le bassin de Graissessac-Lodève (Sud du Massif central): implications tectoniques. C. R. Acad. Sci. Paris, Ser. II 317, 939–945.

Berthé, D., Choukroune, P., Gapais, D., 1979a. Orientations préférentielles du quartz et orthogneissification progressive en régime cisaillant : l'exemple du cisaillement Sud-Armoricain. Bull. Mineralogie 102, 265–272.

Berthé, D., Choukroune, P., Jegouzo, P., 1979b. Orthogneiss, mylonites and non-coaxial deformation of granites: the example of the South Armorican Shear Zone. J. Struct. Geol. 11, 31–42.

Bogdanoff, S., Donnot, M., Ellenberger, F., 1984. Notice explicative. Carte géologique de la France à 1/50 000, feuille Bédarieux (#988) BRGM, Orléans, 105 p.

Bruguier, O., Becq-Giraudon, J.F., Champenois, M., Deloule, E., Ludden, J., Mangin, D., 2003. Application of in situ zircon geochronology and accessory phase chemistry to constraining basin development during post-collisional extension: a case study from the French Massif Central. Chem. Geol. 201, 319–336.

Brun, J.P., Van Den Driessche, J., 1994. Extensional gneiss domes and detachment fault systems: structures and kinematics. Bull. Soc. geol. France 165 (6), 519–530.

Brun, J.P., Sokoutis, D., Van Den Driessche, J., 1994. Analogue modeling of detachment fault systems and core complexes. Geology 22, 319–322.

Buck, W.R., 1988. Flexural rotation of normal faults. Tectonics 7, 959–973.

Davis, G.H., Coney, P.J., 1979. Geologic development of the Cordilleran metamorphic core complexes. Geology 7, 120–124.

Davy, P., Guérin, G., Brun, J.P., 1989. Thermal constraints on the tectonic evolution of a metamorphic core complex (Santa Catalina Mountains, Arizona). Earth Planet. Sci. Lett. 94 (3–4), 425–440.

Demange, M., 1975. Style pennique de la zone axiale de la Montagne noire entre Saint-Pons et Murat-sur-Vèbre (Massif central). Bull. BRGM 2, 269–291.

Gapais, D., 1989. Shear structures within deformed granites: mechanical and thermal indicators. Geology 17, 1144–1147.

Gapais, D., Barbarin, B., 1986. Quartz fabric transition in a cooling syntectonic granite (Hermitage massif, France). Tectonophysics 125, 357–370.

Gasquet, D., Bertrand, J.M., Paquette, J.L., Lehmann, J., Ratzov, G., De Ascenção Guedes, R., Tiepolo, M., Boullier, A.M., Scaillet, S., Nomade, S., 2010. Miocene to Messinian deformation and hydrothermalism in the Lauzière Massif (French Western Alps): new U–Th–Pb and Argon ages. Bull. Soc. geol. France 181, 227–241.

Hurai, V., Paquette, J.L., Huraiová, M., Konečný, P., 2010. U-Th-Pb geochronology of zircon and monazite from syenite and pincinite xenoliths in Pliocene alkali basalts of the intra-Carpathian back-arc basin. J. Volcanol. Geotherm. Res. 198, 275–287.

Jackson, S.E., Pearson, N.J., Griffin, W.L., Belousova, E.A., 2004. The application of laser ablation-inductively coupled plasma-mass spectrometry to in situ U–Pb zircon geochronology. Chem. Geol. 211, 47–69.

Latouche, L., 1968. Contribution à l'étude des Monts de Saint-Gervais. Thèse 3e cycle, université Paris XI-Orsay.

Ludwig, K.R., 1998. On the treatment of concordant uranium-lead ages. Geochim. Cosmochim. Acta 62, 665–676.

Ludwig, K.R., 2001. User's manual for Isoplot/Ex Version 2.49, a geochronological toolkit for Microsoft Excel. Spec Publ., 1a. Berkeley Geochronological Center, Berkeley, USA.

Maluski, H., Costa, S., Echtler, H., 1991. Late Variscan tectonic evolution by thinning of earlier thickened crust. An ^{40}Ar-^{39}Ar study of the Montagne Noire, southern Massif Central, France. Lithos 26, 287–304.

Paquette, J.L., Tiepolo, M., 2007. High resolution (5 μm) U–Th–Pb isotopes dating of monazite with excimer laser ablation (ELA)-ICPMS. Chem. Geol. 240, 222–237.

Pitra, P., Burg, J.P., Schulmann, K., Ledru, P., 1994. Late orogenic extension in the Bohemian Massif: petrostructural evidence in the Hlinsko region. Geodinamica Acta 7, 15–30.

Pitra, P., Ballèvre, M., Ruffet, G., 2010. Inverted metamorphic field gradient towards a Variscan suture zone (Champtoceaux Complex, Armorican Massif, France). J. Metam. Geol. 28, 183–208.

Poilvet, J.C., Poujol, M., Pitra, P., Van Den Driessche, J., Paquette, J.L., 2011. The Montalet granite, Montagne Noire, France: an Early Permian syn-extensional pluton as evidenced by new U-Th-Pb data on zircon and monazite. C. R. Geoscience 343, 454–461.

Roger, F., Respaut, J.P., Brunel, M., Matte, P., Paquette, J.L., 2004. U-Pb dating of Augen orthogneisses from the Axial Zone of the Montagne Noire (southern Massif Central): new witness of Ordovician magmatism into the Variscan Belt. C. R. Geoscience 336, 19–28.

Schärer, U., 1982. The effect of initial ^{230}Th disequilibrium on young U-Pb ages: the Makalu case, Himalaya. Earth Planet. Sci. Lett. 67, 191–204.

Van Den Driessche, J., Brun, J.P., 1989. Un modèle cinématique de l'extension paléozoïque dans le Sud du Massif central. C. R. Acad. Sci. Paris, Ser II 309, 1607–1613.

Van Den Driessche, J., Brun, J.P., 1992. Tectonic evolution of the Montagne Noire (French Massif Central): a model of extensional gneiss dome. Geodinamica Acta 5 (1–2), 85–99.

Wernicke, B., Axen, G.J., 1988. On the role of isostasy in the evolution of normal fault systems. Geology 16, 848–851.

Wiedenbeck, M., Allé, P., Corfu, F., Griffin, W.L., Meier, M., Oberli, F., von Quadt, A., Roddick, J.C., Spiegel, W., 1995. Three natural zircon standards for U–Th–Pb, Lu–Hf, trace element and REE analyses. Geostand. Newslett. 19, 1–23.